View Article Online
DOI: 10.1039/C7NR07819F

Journal Name

ARTICLE

Stable nanoconjugate of transferrin with alloyed quaternary nanocrystals Ag-In-Zn-S as biological entity for tumor recognition

Received 00th January 20xx,
Accepted 00th January 20xx

DOI: 10.1039/x0xx00000x

www.rsc.org/

Edyta Matysiak-Brynda,[a] *Piotr Bujak,*[b] *Ewa Augustin,*[c] *Agata Kowalczyk,*[a] *Zofia Mazerska,*[c] Adam Pron[b] and Anna M. Nowicka[a*]

One way to limit the negative effects of anti-tumor drugs on healthy cells is targeted therapy employing functionalized drug carriers. Here we present a biocompatible and stable nanoconjugate of transferrin anchored to Ag-In-Zn-S quantum dots modified with 11-mercaptoundecanoic acid (Tf-QD) as a drug carrier versus typical anticancer drug, doxorubicin. Detailed investigations of Tf-QD nanoconjugates without and with doxorubicin by fluorescence studies and cytotoxic measurements showed that the biological activity both the transferrin and doxorubicin was fully retained in the nanoconjugate. In particular, the intercalation capabilities of free doxorubicin versus ctDNA remained essentially intact upon its binding to the nanoconjugate. In order to evaluate these capabilities, we studied the binding constant of doxorubicin attached to Tf-QD with ctDNA as well as the binding site size on the ctDNA molecule. The binding constant slightly decreased compared to that of free doxorubicin while the binding site size, describing the number of consecutive DNA lattice residues involved in the binding, increased. It was also demonstrated that QD alone and in the form of nanoconjugate with Tf were not cytotoxic towards human non-small cell lung carcinoma (H460 cell line) and the tumor cell sensitivity of the DOX-Tf-QD nanoconjugate was comparable to that of doxorubicin alone.

Introduction

Nowadays one of the major challenges of medicine is effectively combating diseases of civilization, including cancers, which occupy the second place on the list of causes of mortality from non-communicable diseases.[1,2] Despite the enormous technological and scientific progress, effective methods to combat cancer are still scarce and limited to particular forms of this disease. The difficulty issue of cancer treatment consists of a number of factors, including a plurality of reasons (often not fully identified). This involves, among others: i) significant biochemical similarity of tumor cells *versus* healthy cells, and the resulting low selectivity of therapy and/or ii) high complexity of molecular mechanisms of action described for known therapeutic agents. Drugs applied in chemotherapy of patients often exhibit cytotoxic activity against both tumor and healthy cells.[3,4] This fact is the main driving force of research aimed at reducing / elimination the cytotoxic activity of the anticancer drugs toward the healthy cells. It should be stressed that the targeted transport of a given cytotoxic drug requires the presence of nuclear localization signal (NLS) species (short peptide fragments) which can be easily recognized by the tumor cells.[5-7] Due to the high expression of transferrin receptor 1 (TfR1) in tumor, several times higher than in the case of normal cells, transferrin can be potentially used to deliver cytotoxic agents into malignant cells, including chemotherapeutic drugs.[8,9] Since iron is one of the agents leading to the growth of cancer cells,[10] the presence of transferrin (Tf) can bring a certain risk. For this reason, it is extremely important to prevent the release of iron from the protein structure. The binding constant of iron with transferrin substantially decreases in acidic medium at pH values lower than 6.5,[11] in consequence Fe(III) ions can be more easily liberated from the protein structure.[12-14] This is of crucial importance since the interior of the tumor cells is slightly acidic (pH 4~5).[15] In addition, the iron release process is dependent on many other physicochemical factors such as temperature, presence of chelators and ions, e.g. Cl^- *etc*.

Spherical semiconductor nanocrystals, frequently called "quantum dots" are very attractive nanomaterials for bioimaging applications.[16-18] Several methods of protein anchoring to their surface have been elaborated in recent years.[19,20] However some of these nanocrystals can cause unwanted conformational changes of the anchored proteins.[21,22] These changes can lead to adverse biological side-effects.[23] For this reason the selection of appropriate quantum dots with the goal of obtaining nontoxic conjugates

[a] *Faculty of Chemistry, University of Warsaw, Pasteura 1 Str., PL-02-093 Warsaw, Poland.*
[b] *Faculty of Chemistry, Warsaw University of Technology, Noakowskiego 3 Str., 00-664 Warsaw, Poland.*
[c] *Gdańsk University of Technology, Chemical Faculty, Department of Pharmaceutical Technology and Biochemistry, Narutowicza 11/12 Str., 80-233 Gdańsk, Poland.*
[*] Corresponding authors: anowicka@chem.uw.edu.pl
Electronic Supplementary Information (ESI) available: [details of any supplementary information available should be included here]. See DOI: 10.1039/x0xx00000x

View Article Online
DOI: 10.1039/C7NR07819F

with optimized QD - protein interactions becomes an important goal in all biologically-oriented investigations of their interactions with proteins.[24]

For many years nanocrystals of cadmium selenide (CdSe) have been the subject of the most intensive studies as far as biomedical applications are concerned.[20] A major drawback in the use of these nanocrystals is the surfacial release of free cadmium ions[25] which then are cumulated in living organisms.[26] Intensive research has started few years ago aimed at the preparation of semiconductor nanocrystals, suitable for biomedical applications, which do not contain toxic elements.[27-30] In this respect ternary semiconductor nanocrystals of low bulk band gap such as $CuInS_2$ (Eg = 1.5 eV) and $AgInS_2$ (Eg = 1.8 eV) are of special interest. They can be alloyed with ZnS (Eg = 3.7 eV) or form core/shell systems ($CuInS_2$/ZnS and $AgInS_2$/ZnS) with it. Contrary to their bulk counterparts, these nanocrystals show intensive photoluminescence which is only little dependent on the nanocrystals size. Since their band gap can be controllably tuned by alloying, nanocrystals emitting radiation in the "biological window" spectral range (650 nm to 900 nm), *i.e.* the range where the absorption of the biological background is minimal, can be obtained.[31,32] Aqueous dispersions of core/shell ($CuInS_2$/ZnS, $AgInS_2$/ZnS) and alloyed quaternary (Cu-In-Zn-S and Ag-In-Zn-S) have been used with success both in *in vitro*[33-40] and *in vivo*[32,41-44] biomedical investigations. Nanocrystals used in these applications have to form stable colloidal dispersions in water. There are two strategies in obtaining such nanocrystals. The first one is related to nanocrystals prepared in non-polar solvents and consists of the exchange of primary hydrophobic ligands for hydrophilic ones, followed by their transfer to the aqueous phase. In the second strategy polar solvents are used in the preparation step which results in nanocrystals which can be dispersed in water without the necessity of the ligand exchange. In biological applications bifunctional ligands like 3-mercaptopropionic are frequently used. In this case -SH serves as an anchor group whereas -COOH facilitates the dispersion of nanocrystals in water and serves for grafting biocompatible molecules such as folic acid, for example.

In this research we have exploited a simple method of alloyed, quaternary Ag-In-Zn-S nanocrystals preparation, recently elaborated in our group.[45,46] This method allows for the preparation of large quantities of nanocrystals from simple, commercially available precursors which can be handled in air. In particular, their appropriate alloying leads to quantum dots emitting in the biological window spectral range and showing high photoluminescence quantum yield (≈ 70%). In view of biomedical applications of these nanocrystals we have also elaborated an efficient method of the primary ligands exchange for mercaptoundecanoic acid (MUA) which yields water dispersions of nanocrystals showing the photoluminescence Q.Y of 30%. This is an important point since ligand exchange procedures frequently suffer from a drastic decrease of the photoluminescence.[46]

In the present study we describe the preparation of nanoconjugates of transferrin with alloyed quaternary nanocrystals which can be considered as potential entities for the recognition of tumor cells. It is known that, contrary to the case of carbon-based luminescent nanoparticles, protein-functionalized semiconductor nanocrystals are prone to deactivation processes due to the loss of Fe(III) ions.[47-49] We demonstrate, however, that Ag-In-Zn-S quantum dots modified with 11-mercaptoundecanoic acid are capable of forming biocompatible and stable transferrin-nanoparticle nanoconjugates (Ag-In-Zn-S/MUA-Tf) which fully retained the biological activity of the protein. The synthesized nanoconjugates were qualitatively and quantitatively characterized using complementary techniques such as fluorescence and UV-vis spectroscopy, cyclic voltammetry (CV), thermogravimetric analysis (TGA). Additionally, cytotoxicity of the nanoconjugates and their functionality as drug carriers versus typical anticancer drug, namely doxorubicin, was examined.

Materials and methods

Materials

NaH_2PO_4, Na_2HPO_4, NaCl, KCl (all from POCH, Poland), silver nitrate (99%), indium(III) chloride (98%), zinc stearate (technical grade), 1-dodecanethiol (DDT, 98%), sulfur (99%), 1-octadecene (ODE, 90%), oleylamine (OLA, 70%), 11-mercaptoundecanoic acid (MUA, 95%), dimethyl sulfoxide (DMSO), human transferrin (Tf), apo-transferrin (apo-Tf), doxorubicin hydrochloride (DOX), glutaraldehyde solution, 3-(4,5-dimethylthiazol-2-yl)-2,5-diphenyltetrazolium bromide (MTT) and calf thymus double stranded DNA (ctDNA) were all purchased from Sigma. Reagents and chemicals used in the nanoconjugate synthesis and in the cytotoxicity tests were of the highest purity available and used as received. All solutions were prepared in 0.02 M PBS buffer with addition of 2 mM KCl and 150 mM NaCl, pH 7.4.

Synthesis of transferrin-nanoparticle nanoconjugate and doxorubicin-transferrin-nanoparticle nanoconjugate

Preparation of Ag-In-Zn-S nanocrystals. In the synthesis of Ag-In-Zn-S nanocrystals and primary ligands exchange procedures earlier described in literature were followed.[45] All operations were carried out under constant dry argon flow. Silver nitrate (0.03 g, 0.17 mmol), indium(III) chloride (0.13 g, 0.59 mmol), zinc stearate (0.40 g, 0.63 mmol), and DDT (0.20 g, 1.00 mmol) were mixed with ODE (15 mL) in a three-neck flask. The mixture was heated to 150 °C until a homogeneous solution was formed. Then sulfur (0.015 g, 0.47 mmol) dissolved in 1 mL of OLA was quickly injected into the reaction solution. The temperature was increased to 180 °C, and the mixture was kept at this temperature for 60 min. After the mixture was cooled to room temperature, toluene (20 mL) was added, and the reaction mixture was centrifuged - the isolated black precipitate was separated. The supernatant was treated with 30 mL of acetone leading to the precipitation of the desired fraction of nanocrystals. The nanocrystals were separated by centrifugation (7000 rpm, 5 min) and then redispersed in toluene.

View Article Online
DOI: 10.1039/C7NR07819F

Ligand exchange for 11-mercaptoundecanoic acid (QD). A mixture of MUA (0.5 g, 2.3 mmol) and NaOH (0.1 g, 2.5 mmol) in water (10 mL) was stirred and heated at 50 °C until a homogenous solution was formed. Then toluene dispersion (5 mL) of nanocrystals prepared as described above was injected into this solution. The as-obtained two-phase mixture was heated at 80 °C for 8 h under an argon atmosphere. After cooling the reaction mixture was centrifuged to obtain complete phase separation - solids and the organic phase were discarded. Water solution was then mixed with 20 mL of acetone which led to the precipitation of nanocrystals. After centrifugation, the nanocrystals were redispersed in 10 mL of water.

Anchoring of transferrin to QD nanocrystals. In the preparation of the transferrin-semiconductor nanoconjugate (Tf-QD), a mixture of QD (1.0 mg·mL^{-1}) and Tf (0.2 mg·mL^{-1}) was incubated for 1 h at room temperature. During this step, the mixture was continuously stirred using a thermomixer. In these conditions the Tf-QD nanoconjugates are readily formed despite the fact that at pH 7.4 QDs are negatively charged due to the presence of carboxylic groups on their surface and the isoelectric point of Tf molecules is 5.2, also imposing a net negative charge on this moiety.[50,51] However, Tf contains Fe(III) ions which have high binding affinity to MUA carboxylic groups. The synthesized Tf-QD nanoconjugate (step I in Scheme 1) was washed several times with small portions of acetone to remove unreacted Tf, then dried in a desiccator and finally dispersed in 0.02 M PBS buffer, pH 7.4. Then, it was used as a doxorubicin drug carrier. Doxorubicin was covalently conjugated to Tf (DOX-Tf-QD; step II in Scheme 1) by the formation of a Schiff base in a cross-linking reaction with glutaraldehyde.[52]

Cell culture

Non-small cell lung carcinoma, human H460 cell line was obtained from ATCC (American Type Culture Collection) and was tested negatively for mycoplasma using Universal Mycoplasma Detection Kit, ATCC-30-1012K (ATCC). Cells were grown in RPMI 1640 medium (Sigma-Aldrich, St Louis, MO, USA) supplemented with 10% heat-inactivated fetal bovine serum and antibiotics (100 µg·mL^{-1} streptomycin, 100 U·mL^{-1} penicillin), in a 5% CO_2 atmosphere at 37 °C. Under these growth conditions the cell-doubling time was approximately 18 h. All experiments were performed with the cells in the exponential phase of growth.

Cytotoxicity assessment

Cell viability was measured by MTT (3-(4-5-dimethylthiazol-2-yl)-2,5-diphenyltetrazolium bromide, Sigma-Aldrich, St Louis, MO, USA) assay. Cells (2x10^4/well) were seeded on 24-well plates and exposed to different concentrations of QD, Tf-QD, apo-Tf-QD, DOX-QD, DOX-Tf-QD, DOX-apo-Tf-QD and Dox unbound for 72 h. At the end, 0.5 mg·mL^{-1} MTT was added to each well and then incubated for 3 h at 37 °C. The medium was removed and crystals of formazan were dissolved in DMSO. Finally, the absorbance was measured at 540 nm using a microplate reader (iMarkTM, Bio-Rad, Hercules, CA, USA).

Scheme 1. Scheme of preparation of nanoconjugates: Tf-QD and DOX-Tf-QD.

The cytotoxic effect of treatment with drugs was expressed as the IC_{50} value (drug concentration required to inhibit cell

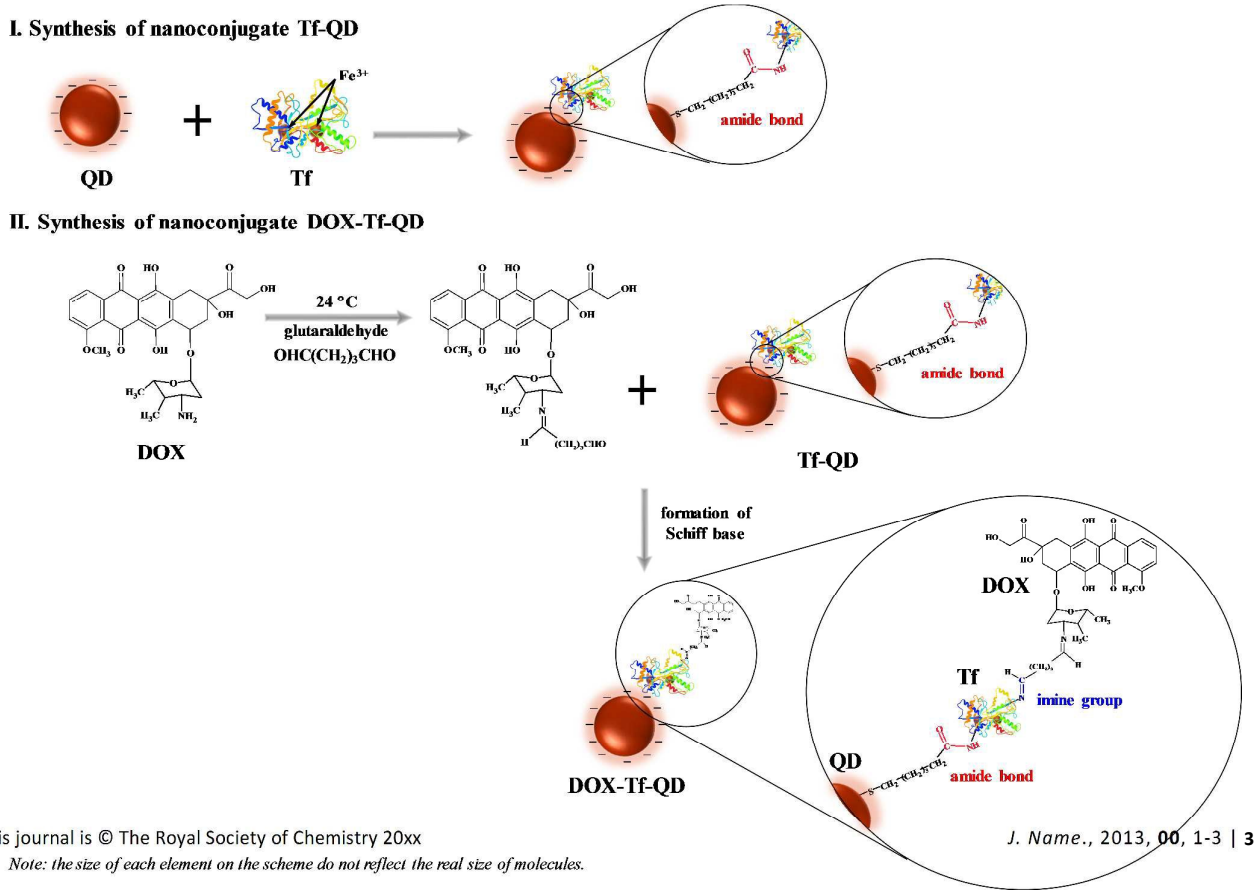

Note: the size of each element on the scheme do not reflect the real size of molecules.

View Article Online
DOI: 10.1039/C7NR07819F

growth by 50% compared to untreated control cells). Results were obtained in three independent experiments (n=3).

Applied characterization methods

X-ray diffraction patterns were recorded on a Seifert HZG-4 automated diffractometer using Cu $K_{1,2}$ radiation (1.5418 Å). The data were collected in the Brag-Brentano ($\theta/2\theta$) horizontal geometry (flat reflection mode) between 10° and 70° (2θ) in 0.04° steps, at 10 s $step^{-1}$. The optics of the HZG-4 diffractometer was a system of primary Soller slits between the X-ray tube and the fixed aperture slit of 2.0 mm. One scattered-radiation slit of 2 mm was placed after the sample, followed by the detector slit of 0.2 mm. The X-ray tube operated at 40 kV and 40 mA. TEM analysis were performed on a Zeiss Libra 120 electron microscope operating at 120 kV. The elemental analysis was carried out with a multichannel Quantax 400 EDS system with 125 eV xFlash Detector 5010, Bruker using 15 kV electron beam energy.

FTIR spectroscopy and dynamic light scattering (DLS) measurements were used to confirm the successful conjugation of transferrin to QD and DOX to the nanoconjugate. In the case of FTIR measurements the pellets were prepared from a mixture of 300 mg of spectrally pure KBr and *ca*. 0.8-1.2 mg of the nanoconjugates (Tf-QD, DOX-QD, DOX-Tf-QD) and pure components (QD, DOX and Tf). The spectra were acquired in a transmission mode on Perkin Elmer System 2000 spectrophotometer with the spectral resolution of 4 cm^{-1}. In turn, the DLS measurements were performed with a Zetasizer nano series apparatus (Malvern) with a He-Ne (4 mW) laser at 632.8 nm. DLS measurements were carried out in water at 21 °C, at least five times, with three freshly prepared samples.

To monitor the possible release of Fe from Tf molecules, as a result of conjugation process with QD, CD and UV-vis techniques were applied. The CD spectra were obtained with a J-815 circular dichroism spectrometer (Jasco) applying the following parameters: scanning speed 100 $nm{\cdot}min^{-1}$, data pitch 0.5 nm and spectral bandwidth 2 nm. A quartz cuvette of 1-cm length was used as the optical window. The absorption spectra were recorded using a PerkinElmer spectrometer, model Lambda 25, at temperature 21 °C in the same cuvette as that used for CD measurements.

Thermogravimetric analysis (TGA) was carried out on a TGA Q50 apparatus (TA Instruments). The TGA measurements were performed under nitrogen blanket with a heating rate of 10 $°C{\cdot}min^{-1}$. These measurements were performed with the goal to determine the amount of Tf grafted to the nanocrystals surface and in the next step the amount DOX to attached to the Tf-QD nanoconjugate.

Cyclic- and differential pulse voltammetry studies were performed using an Autolab, model PGSTAT 12 potentiostat equipped with an ECD amplifier module. The voltammetric measurements were performed in the three-electrode configuration with a glassy carbon working electrode, GCE, (ϕ = 3 mm, BAS Instruments), an Ag/AgCl reference electrode and a platinum wire serving as the auxiliary electrode. The surface of the working electrode was polished with 1 µm Al_2O_3 powder on a wet pad. After each polishing, the electrode was rinsed with direct stream of ultrapure water (Hydrolab) with the goal to completely remove alumina from its surface.

Fluorescence spectra were recorded on a Scinco FluoroMate FS-2 spectrofluorimeter using λ_{exc} in the range 300 - 900 nm, 1 nm slit and the scan rate of 600 $nm{\cdot}min^{-1}$. The studied colloidal solutions were placed in a 1 cm thick quartz cuvette.

Results and discussions

Characteristic of Ag-In-Zn-S/MUA (QD)

Alloyed Ag-In-Zn-S used in this research were prepared using *hot-injection* through injection of a solution of sulfur in OLA to a mixture of metals precursors and DDT dissolved in ODE.[45,46] Starting from the molar ratio of metal precursors Ag/In/Zn=1.0/3.5/3.6 nanocrystals of the following composition were obtained $Ag_{1.00}In_{3.10}Zn_{1.00}S_{4.00}$, as determined from EDS studies (see Fig. S1, in ESI for the representative spectra). In Fig. 1A and B TEM images of the nanocrystals capped with initial ligands and with MUA are presented, showing essentially the same spherical shape of the average diameters equal to 5.8±0.9 nm and 5.8±1.1 nm, respectively. The powder diffractogram of nanocrystals capped with primary ligands is show in Fig. 1A as an inset. The positions of the recorded reflections are intermediate between these characteristic of orthorhombic $AgInS_2$ (JCPDS 00-025-1328) and those of cubic ZnS (JCPDS 00-05-0566) which clearly confirms the alloyed structure of the obtained nanocrystals. Using the procedure described in the literature[46,53] amines and carboxylates were identified as primary ligands in these nanocrystals. These ligands are rather weakly bound to the nanocrystals surface, contrary to the case of thiol-type ligands. As a result their exchange for 11-mercaptoundecanoic acid ligands is very efficient and stable colloidal dispersions in water can be obtained.[46] One should however note that the ligand exchange process significantly changes the composition of the nanocrystals, lowering the content of indium and yielding nanocrystals of the following

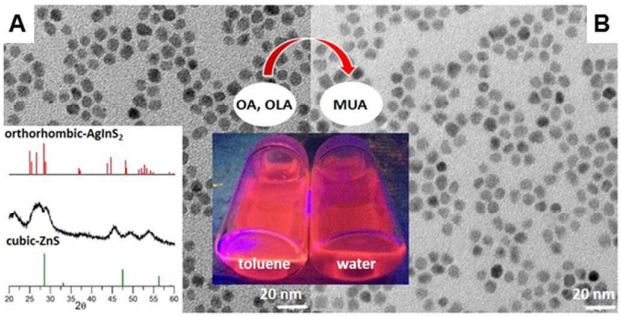

composition $Ag_{1.00}In_{0.97}Zn_{1.05}S_{3.50}$, still retaining high photoluminescence quantum yields of *ca*. 30%.[46]

Fig. 1 TEM images of Ag-In-Zn-S quaternary nanocrystals before (A) and after (B) the exchange of initial capping ligands for 11-mercaptoundecanoic acid. The inset panel in (a) shows

View Article Online
DOI: 10.1039/C7NR07819F

the XRD pattern of Ag-In-Zn-S nanocrystals capped with initial ligands.

Evidence of QD and Tf interactions through QD fluorescence quenching studies

Before detailed characterization of Tf-QD it is instructive to investigate the interactions of "free" transferrin with the nanocrystals. This can be conveniently done by the investigations of QDs fluorescence quenching induced by the presence of Tf in the studied solution.

Fig. 2A shows gradual decrease of MUA-capped quantum dots fluorescence with increasing concentration of Tf in the solution. In particular, for the highest Tf content (2 μM), the fluorescence intensity is quenched to *ca.* 40% of its originalvalue. A control experiment, carried out with apo-Tf (*i.e.* transferrin without Fe^{3+} ions) in the same concentration range, showed only minimal decrease of the QDs fluorescence in the presence of apo-Tf (see inset in Fig. 2A). This finding clearly proves that the quenching process is directly connected with the presence of iron(III) ions in the investigated protein.

The Tf-QD interactions can be quantitatively described by the quenching constant (K_{SV}) of the Tf-QD nanoconjugate according to the Stern-Volmer equation:[54-56]

$$\frac{I_0}{I} = 1 + K_{SV} \cdot C_{Tf} \qquad (1)$$

where C_{Tf} is the molar concentration of transferrin, I_o and I are the fluorescence intensity of QD in the absence and in the presence of Tf, respectively.

K_{SV} calculated from the slope of the plot I_o/I = f(C_{Tf}) was equal to $(7.05 \pm 0.6)\cdot 10^5$ M^{-1}. The Stern-Volmer plots for both cases (*i.e.* QD-Tf and QD-apo-TF interactions) are linear (see Fig. 2B), indicating that only one type of quenching process occurs, either static or dynamic one.[57,58] Static and dynamic quenching can be distinguished by monitoring the changes in the quenching constant values as a the function of temperature and viscosity, or the lifetime of the fluorophore in the absence and in the presence of a quencher.[57] An increase of the K_{SV} value with temperature indicates the dynamic quenching. Oposite behavior of K_{SV} *vs*. *T*, is, in turn, characteristic of static quenching. With increasing temperature the value of the quenching constant decreased, so in the studied case the static quenching took place and, subsequently, the quenching constant could be considered as the association constant. A similar type of the static quenching mechanism was earlier observed for a variety of protein-nanoparticle nanoconjugates.[23,24]

Secondary structure of Tf inTf-QD nanoconjugate

Circular dichroism (CD) is a very powerful method for the determination of proteins secondary structure. The positions of the diagnostic bands give precise information concerning the content of α-helices, β-sheets, turn and random coil in the structure of a given protein.[59] The CD spectrum (dashed line in Fig. 2C) of native transferrin exhibits a negative band at 209 nm and a weak shoulder around 220 nm. The secondary structure analysis of Tf shows that α-helix constitutes around 20% of the protein structure whereas β-sheet - around 60%. This finding is in good agreement with the literature data.[60] Upon formation of Tf-QD nanoconjugate (solid line in Fig. 2C) the β-sheet content increases on the expense of α-helix structure.

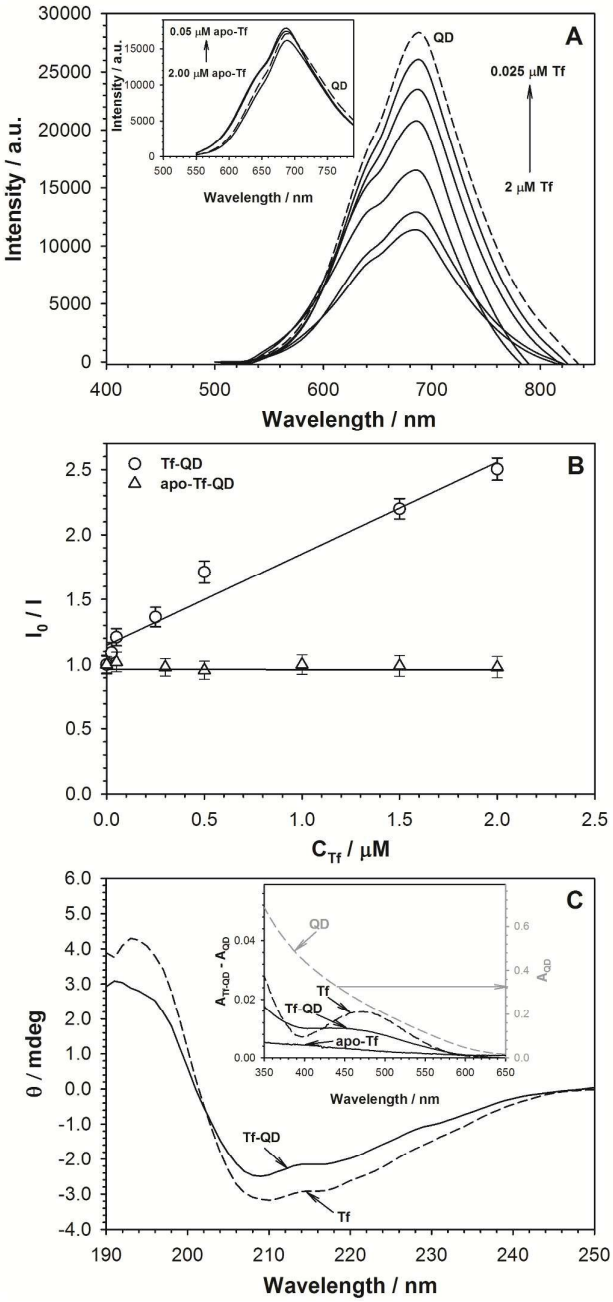

Fig. 2 (A) Fluorescence quenching of QD by Tf in 0.02 M PBS buffer of pH 7.4. Inset: Fluorescence quenching of QD by apo-Tf. Experimental conditions: C_{QD} = 1 mg·mL^{-1}; C_{Tf} = 0.025; 0.05; 0.25; 0.5; 1.5 and 2 μM. (B) Stern-Volmer plots of QD quenching fluorescence as a function of Tf and apo-Tf concentrations. Other experimental conditions as in Fig. 2A. (C) CD spectra of the pure transferrin and Tf-QD nanoconjugate. Inset: UV-vis spectra of apo-Tf, Tf, QD and nanoconjugate Tf-QD. Experimental conditions: C_{Tf} =

View Article Online
DOI: 10.1039/C7NR07819F

5 μM, C_{QD} = 1 mg·mL^{-1}, $C_{Tf\text{-}QD}$ = 50 μg·mL^{-1}, $C_{apo\text{-}Tf}$ = 5 μM; 0.02 M PBS buffer of pH 7.4.

Moreover, the maximum at 193 nm shifts to shorter wavelengths, additionally confirming the increase of the β-sheet content. These results clearly indicate that only negligible conformational alterations in the secondary structure of Tf take place upon transferrin grafting to QDs.

UV-vis spectroscopy is the best method to confirm that, despite of the slight conformation changes of Tf after conjugation, iron is not released from the protein shell upon transferrin conjugation to QDs. A clear band at *ca*. 470 nm in the spectra of Tf and Tf-QD (see inset in Fig. 2C) unequivocally prove that iron cations are retained in the protein structure, since this band is absent in the spectrum of apo-Tf.

Characterization of transferrin-functionalized Ag-In-Zn-S nanocrystals

Mercaptoundecanoic acid (MUA) binds to the nanocrystal surface via its thiol group, the carboxylic group assures, in turn, the stabilization of the colloidal dispersions of these nanocrystals in water. Transferrin readily binds to QD-MUA to yield Ag-In-Zn-S/MUA-Tf (Tf-QD). In this hybrid the Ag/Fe ratio was 1.000/0.025 with essentially no change in the composition of the inorganic core after Tf binding ($Ag_{1.00}In_{1.06}Zn_{1.07}S_{3.04}$ vs $Ag_{1.00}In_{0.97}Zn_{1.05}S_{3.50}$ before Tf anchoring, see Fig. S1, ESI). Taking into account the nanocrystals composition and the size of their inorganic core (5.77 ± 1.15 nm) it can be calculated that one individual nanocrystals binds, on the average, 5 transferrin molecules (see ESI).

To confirm the stoichiometry of the nanoconjugate the Job plot was constructed by investigating the fluorescence quenching process. The Job's plot presented in Fig. S2 in ESI shows a maximum that appears at a volume fraction for x_{Tf} = 0.83 ($x_{Tf} = V_{Tf} / (V_{Tf} + V_{QD})$). In this experiments the solutions containing pure Tf and QD was in the same concentration (mg·mL-1). Taking into account the molecular weight of a single QD functionalized with MUA (MW_{QD} = ~653 878 g·mol^{-1}) and Tf protein (MW_{Tf} = 79 985 g·mol^{-1}) and convert the mass ratio to molar one the stoichiometry of the QD – Tf reaction is 1:40. It indicates that the number of Tf molecules attached to one QD nanocrystal estimated from Job plot is 8 times higher than the molar ratio determined from EDS data (5 (Tf) : 1 (QD)). It should be stressed that the EDS measurements, due to the EDS technique sensitivity, were performed with iron saturated transferrin (Tf-Fe_2), since the Job plot was constructed on the basis of the experiments done for human transferrin (containing mainly monoferric transferrin, Tf-Fe). The disagreement in the moles of Tf molecules bounded to one QD nanocrystal calculated from Job plot and EDS data is a consequence of the Tf molecules size, which strongly depends on the presence of iron in protein structure. It is known that the dimension of Tf molecule increases with an increase of the iron saturation level.[61] Taking into account that the size of Tf-Fe is insignificant higher than apo-Tf the number of Tf-Fe molecules attached to one QD nanocrystal can be from 3 to 8 times higher than Tf-Fe_2. The possible arrangement of Tf-Fe and Tf-Fe_2 molecules on QD surface schematically is shown in Figure 3.

The way of transferrin binding to QDs was checked by FTIR.

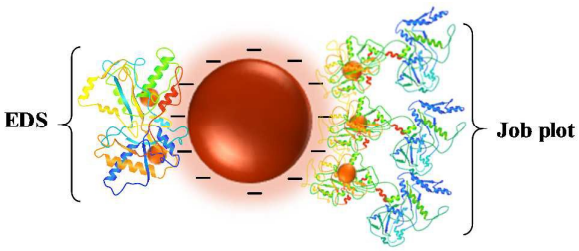

Representative FTIR spectra of QD, Tf and nanoconjugate Tf-QD

Fig. 3 Scheme of possible arrangement of Tf-Fe and Tf-Fe_2 molecules on QD nanocrystal surface.

are presented in right inset of Fig. 4A. The FTIR spectrum of pure Tf exhibits two strong bands at ca. 1650 and 1530 cm^{-1} which correspond to amide I (C=O stretching vibration) and amide II (N-H bending and C-N stretching vibrations), respectively.[62-64] After the conjugation of Tf with QD the intensity of these bands decrease compared to pure Tf. It should be noted that the decrease of the intensity of amide II band is higher than amide I band. This diminishing is due to the fact that the N-H groups of protein take part in the formation of the amide bonds between Tf and QD. Additionally the conjugation process of Tf with QD via amide bond leads to bathochromic shift by ca. 20 cm^{-1} and broaden of the band. These all phenomena can be considered as a spectroscopic manifestation of Tf covalent binding to ligand-capped QDs. Doxorubicin, in turn, is covalently attached to nanoconjugate Tf-QD by the formation of a Schiff base in the cross linking process using glutaraldehyde, again confirmed by FTIR spectroscopy. Schiff base compounds have characteristic band at ca. 1640 cm^{-1}, associated with the –C=N stretching vibration, which indicating the presence of the newly formed imine linkage.[65-69] The evidence for imine-bond formation during the DOX conjugation to Tf-QD results in band broadening and shifting towards higher wavenumbers. The presence of DOX in DOX-Tf-QD gives rise to several IR spectral features characteristic of this drug (Fig. 4A). In particular, the carboxylate band at *ca*. 1380 cm^{-1} of the DOX-Tf-QD is hyprochromically shifted, similarly as the amide II band as compared to the corresponding band in Tf-QD. Again, these features can be considered as a spectroscopic manifestation of the covalent bonds between TF-QD and the carboxylate group of doxorubicin. The presence of the bands in the range from 1000 and 1250 cm^{-1} additionally confirms successful attachment of doxorubicin. In the absence of Tf on the surface of QD, doxorubicin can also be covalently attached to QD *via* amide bond, which is well identified by the presence of diagnostic bands in the FTIR spectrum of DOX-QD (see the left inset in Fig. 4A).

View Article Online
DOI: 10.1039/C7NR07819F

The successful of conjugation process between Tf and QD and DOX to the Tf-QD nanoconjugate was also confirmed by dynamic light scattering (DLS) investigations. The obtained data showed the following sequence of hydrodynamic diameters: 9.10 ± 0.81, 12.80 ± 1.2, 9.62 ± 1.02, 13.13 ± 0.68 and 10.57 ± 0.53 nm for QD, Tf-QD, apo-Tf-QD, DOX-Tf-QD and DOX-apo-Tf- QD, respectively. This sequence clearly confirmed that DOX was successfully anchored to the Tf-QD nanoconjugate.

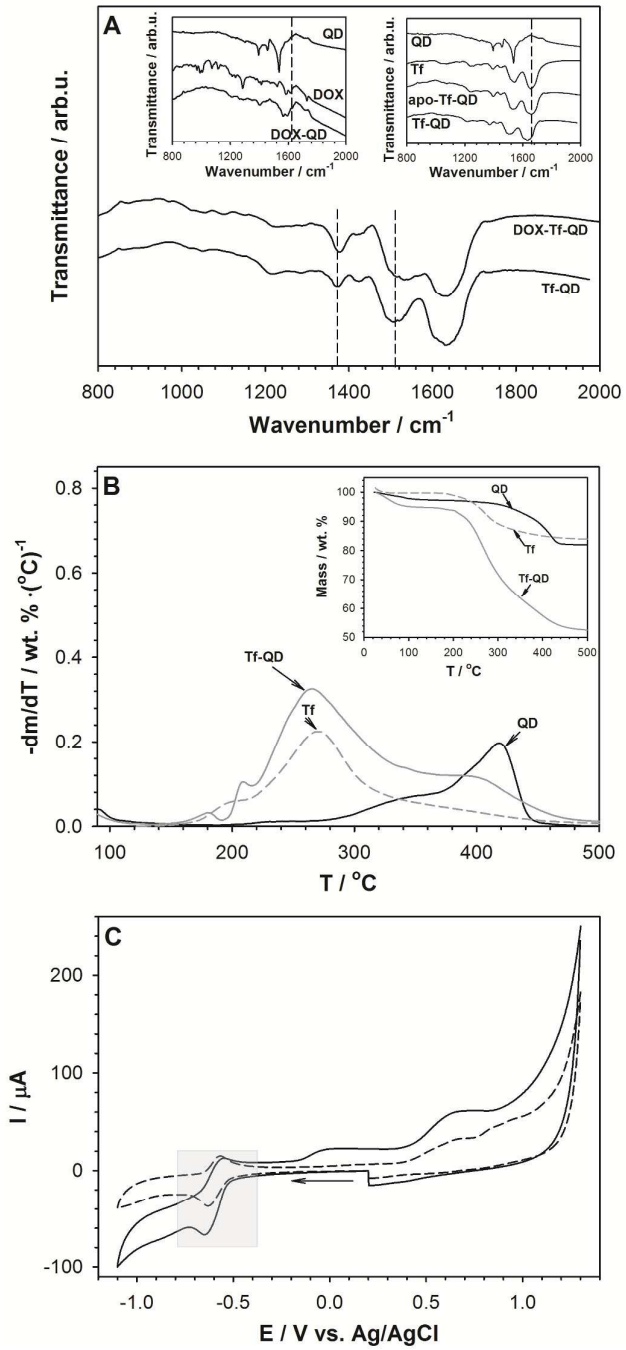

Fig. 4 (A) FTIR spectra of QD, DOX, TF and nanoconjugates DOX-QD, Tf-QD and DOX-Tf-QD. (B) TGA curves and their first derivatives of free components: Tf, QD and nanoconjugate Tf-QD. (C) Cyclic voltammograms obtained for doxorubicin (dashed line) and nanoconjugate DOX-Tf-QD adsorbed at the electrode surface (solid line). Experimental conditions: C_{DOX} = 5 µM, $C_{DOX\text{-}Tf\text{-}QD}$ = 50 µg·mL^{-1}; 0.02 M PBS buffer of pH 7.4; GC electrode ϕ = 3 mm.; scan rate: 100 mV·s^{-1}.

Clear evidence of transferrin binding to MUA modified nanocrystals can be obtained from the TGA studies. In Fig. 4B TG plot of MUA capped nanocrystals (QD) is compared with the corresponding mass loss curves of Tf-QD. The TG curves registered for pure TF can be divided into two parts. The first part corresponds to the temperature range of 21 - 100 °C with the mass loss of *ca.* 6% corresponding to the desorption of water molecules and possibly some weakly bound ligands. The thermal decomposition of pure transferrin starts at 160 °C and reaches the highest rate at *ca.* 270 °C. The decomposition continues at higher temperatures, however at significantly lower rates. QD-MUA are more temperature resistant and start to decompose at 280 °C, reaching the highest decomposition rate at 420 °C. Above 450 °C no further mass loss can be observed. In the nanoconjugate the mass losses are more pronounced than in the case of separated nanoconjugate components exceeding at 500 °C 40% of the nanoconjugate original mass. Evidently, both nanoconjugate components mutually catalyze their decomposition. The differential TG curves give a clear evidence for the nanoconjugate formation since in the registered differential curve of the nanoconjugate features originating from both components can be identified.

The amounts of doxorubicin bound to the QD and to the Tf-QD nanoconjugate were determined from the charge under the cathodic peak at the potential *ca*. –0.6 V present in the cyclic voltammograms of DOX-QD and DOX-Tf-QD (see Fig. 4C). Assuming a two electron process (z = 2), using the Faraday formula ($m_{DOX} = Q_{DOX}\cdot M_{DOX} / z\cdot F$) the estimated mass of DOX was *ca*. 41 mg and 81 mg per 1 g of QD (m_{DOX} / $m_{QD\ used\ in\ synthesis}$) and 1 g of Tf-QD nanoconjugate (m_{DOX} / $m_{Tf\text{-}QD\ used\ in\ synthesis}$), respectively. It should be noted, that this number corresponds to *ca*. 60% of maximal value, most likely represents the lower limit of surface coverage, as we believe that not all doxorubicin can participate in the redox process. It is probably because of steric reasons, where some doxorubicin molecules can be screened from the electrode surface. All calculations are given in ESI.

ctDNA interactions with Tf-QD nanoconjugate

The action of the most of the cytostatic drugs is based on their interactions with DNA, so it was very important to check the influence of Tf-QD nanoconjugate on the conformational changes in the ctDNA structure. The UV-vis spectroscopic study (see Fig. 5A) revealed that the intensity of the absorption peak characteristic of DNA at 260 nm slowly grew with increasing concentration of Tf-QD nanoconjugate. The resulting maximal absorbance registered for Tf-QD concentration 0.15 mg·mL^{-1} reached a value by 17% higher

View Article Online
DOI: 10.1039/C7NR07819F

than that measured for the solution with no Tf-QD added. No changes in the position of this absorbance band were observed, which indicated that structural alterations of ctDNA were limited to the local loosening of the DNA double helix.

To estimate the influence of the Tf-QD nanoconjugate on the ctDNA structure voltammetric studies were also carried out with ctDNA accumulated at the glassy carbon surface.The experiments were performed at a constant potential +0.08 V in the ctDNA-containing buffer (39 μM base pairs; 10 minutes). The calculated total surface concentration of ctDNA adsorbed at a GC electrode surface was equal to $2.05 \cdot 10^{-11}$ mol·cm^{-2}.

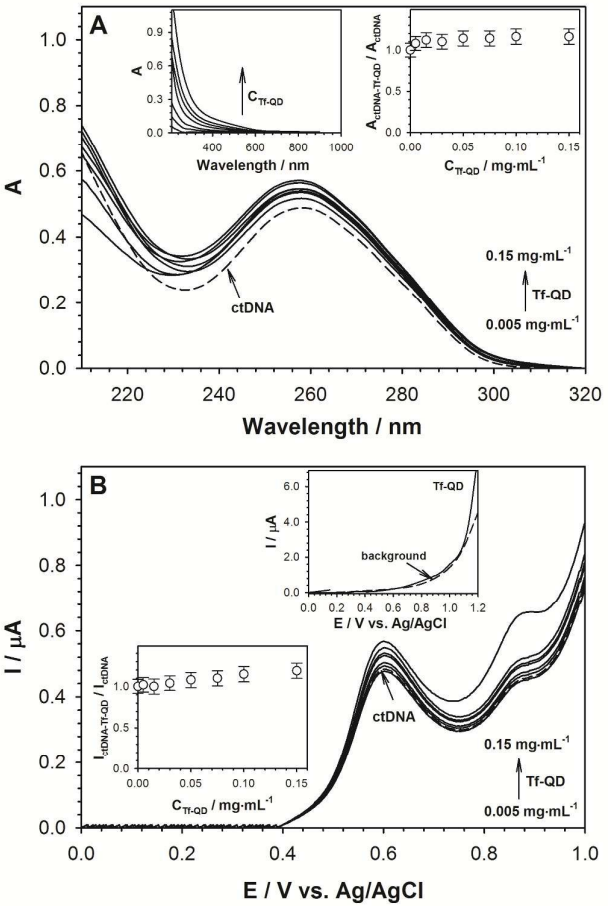

Fig. 5 (A) Changes in UV-vis spectra of ctDNA induced by its interaction with Tf-QD nanoconjugate of various concentrations. Left inset: UV-vis spectra of Tf-QD nanoconjugate. Right inset: Dependence of the relative DNA absorbance intensity at 260 nm versus concentration of Tf-QD. (B) DP voltammograms of ctDNA registered in the presence of Tf-QD nanoconjugate of various concentration. Upper inset: DP voltammograms of the background and Tf-QD nanoconjugate. Bottom inset: Dependence of the relative ctDNA oxidation current intensity at *ca*. 0.6 V versus concentration of Tf-QD. Experimental conditions: C_{Tf-QD} = 0.005; 0.015; 0.03; 0.05; 0.075; 0.10 and 0.15 mg·mL^{-1}; 0.02 M PBS buffer of pH 7.4, GC electrode ϕ = 3 mm.

The obtained DP voltammetric curves (see Fig. 5B) reveal the existence of two peaks: at *ca.* 0.60 V and *ca.* 0.88 V which correspond to the oxidation of guanine and adenine, respectively.[70,71] The presence of Tf-QD nanoconjugate leads to a slight increase (by less than 20%) of the oxidation current. This fact suggests that the oxidation damage of DNA (including the formation of oxidized bases lesions) did not take place. More specifically, local loosening of DNA double helix, already evidenced by UV-vis spectroscopy, facilitates the oxidation process.

Application of Tf-QD nanoconjugate as a doxorubicin carrier

Since transferrin can be potentially used for cytotoxic agents delivery into malignant cells we have decided to test the Tf-QD nanoconjugate as an anticancer drug carrier. Therapeutic properties of the majority of anticancer drugs are related to their interactions with ctDNA. In this part of our studies we used popular anticancer drug, doxorubicin (DOX). The anticancer

action of DOX is related, among others to its non-covalent binding to dsDNA, which causes the inhibition of replication process leading to cell death.[72,73] The interactions between free DOX and dsDNA as well as DOX incorporated into the Tf-QD nanoconjugate and dsDNA can be characterized by the determination of the binding constant (K) and the number of binding site sizes (n).[74,75] It is known that doxorubicin binds with dsDNA mainly by intercalative base-stacking and electrostatic interactions at the minor groove,[76] therefore it is interesting to find out how the DNA-binding properties of doxorubicin and cytotoxicity towards tumor cells are affected by its anchoring to the Tf-QD nanoconjugates. The binding parameters of the interactions of DOX conjugated with Tf-QD and ctDNA were calculated from the UV-vis spectroscopic data. The polymer model of McGhee and von Hippel was used for this purpose.[77] The following formula describes the interactions between the ctDNA strand and the ligand:

$$\frac{r}{C_f} = K_b(1-nr)\left[\frac{1-nr}{1-(n-1)r}\right]^{n-1} \qquad (2)$$

where K_b is the binding constant, n is the number of binding matrix units (base pairs) that are occupied by one molecule of the drug, and $r = C_b/C_{matrix}$ unite, where $C_b = C_o - C_f$, C_b is the concentration of the drug molecules bound to ctDNA, C_o is the total concentration of the drug, C_f is the concentration of the free molecules of the drug in the solution, and C_{matrix} unite is the analytical concentration of the binding unit in ctDNA. The changes of the binding parameters of free DOX and DOX-Tf-QD with ctDNA are presented in Table 1. These results indicate that the presence of QD, Tf and Tf-QD do not affect the binding activity of DOX versus DNA. The Kb values of DOX conjugates with DNA are ~2 times smaller than those determined for free ctDNA-DOX, while the number of binding DNA units increase from 2.9 to 10 in the presence of Tf and Tf-QD nanoconjugate. The determined interactions parameters show that it is possible to monitor the cytotoxicity properties of DOX conjugated with Tf-QD.

View Article Online
DOI: 10.1039/C7NR07819F

Nanoconjugates	K_b ± SD / M^{-1}	n ± SD
ctDNA-DOX	$(4.5 \pm 0.4)\cdot10^5$	2.9 ± 0.8
ctDNA-DOX-Tf	$(3.2 \pm 0.6)\cdot10^5$	5.7 ± 1.3
ctDNA-DOX-QD	$(3.6 \pm 0.5)\cdot10^5$	3.5 ± 0.4
ctDNA-DOX-Tf-QD	$(2.2 \pm 0.8)\cdot10^5$	10.2 ± 1.8

Table 1 Interactions parameters between free DOX and DOX in different types of conjugates and ctDNA at room temperature and pH 7.4.

Cytotoxicity of the studied nanoparticles against tumor cells

In order to evaluate the potency of the studied nanoparticles against tumor cells we selected human non-small cell lung carcinoma, H460 cell line, because lung tumors belong to the most popular and difficult for therapy in human. Cytotoxicity against H460 cells was determined with MTT assay following 72 h of incubation with nanoconjugate Tf-QD, nanoconjugate DOX-Tf-QD and free doxorubicin. IC_{50} value (concentration that yielded 50% cell growth inhibition, Fig. 6A) was applied as the measure of nanoparticle cytotoxicity. After a continuous 72 h exposure, nanoconjugate DOX-Tf-QD caused a concentration-dependent inhibition of growth of H460 lung carcinoma cells (Fig. 6B). Interestingly, nanoconjugate Tf-QD without doxorubicin did not influence the growth of H460 tumor cells (Fig. 6C). In conclusion, we showed that doxorubicin-transferrin-nanoparticle conjugates exhibited the significant growth inhibition of H460 tumor cells comparable to that observed after treatment of free doxorubicin. Our future studies should propose the mechanism of cell penetration of this doxorubicin conjugate and biological effects induced. We consider the lysosome-endosome nanoparticle-drug conjugates penetrating the cells,[78,79] what would result in apoptosis.[80]

Conclusions

Tumor cells have a large number of transferrin receptors on the surface of their cytoplasmic membranes, many times greater than in healthy cells. This fact of overexpression of transferrin receptors has made it possible to support the selective transport of anticancer drugs. Ag-In-Zn-S quantum dots in complex with transferrin, offer exciting new opportunities toward developing new effective drug delivery systems. On the basis of the fluorescence spectroscopy studies, it can be concluded that transferrin forms a stable complex with Ag-In-Zn-S quaternary quantum dots, but only if iron(III) ions are present in its structure. The fluorescence as well as DLS experiments with transferrin (containing Fe(III) ions) and apo-transferrin (without Fe(III) ions) showed that amide bond between –COOH groups of QD and $–NH_2$ of Tf is formed. Electrostatic interactions between carboxylic groups of surfacial ligands and positively charged iron ions of Tf are vital for the covalent bond formation since this process does not occur between iron free apo-Tf and QDs. The formation of amide linkages were confirmed by IR spectroscopy.

Functionality of the proposed Tf-QD as a drug carrier was tested *versus* doxorubicin, the standard anticancer drug. The activity of this drug is apparently related to its direct interactions with ctDNA. The performed experiments clearly proved that after binding to the Tf-QD nanoconjugate, the DOX molecules are still capable of intercalating the ctDNA helixes. Spectroscopic results show that the intercalation behavior of DOX in the complex with Tf-QD is preserved. Moreover, it was demonstrated that Tf-QD itself were not cytotoxic against human non-small cell lung carcinoma (H460 cell line) at wide range of concentrations, whereas DOX-Tf-QD nanoconjugate reached cytotoxicity comparable to that of DOX alone.

A

Nanoconjugates	IC_{50} ± SD [μM]
DOX-QD	0.164 ± 0.03
DOX-Tf-QD	0.131 ± 0.03
DOX-apo-Tf-QD	0.115 ± 0.01
DOX	0.127 ± 0.05

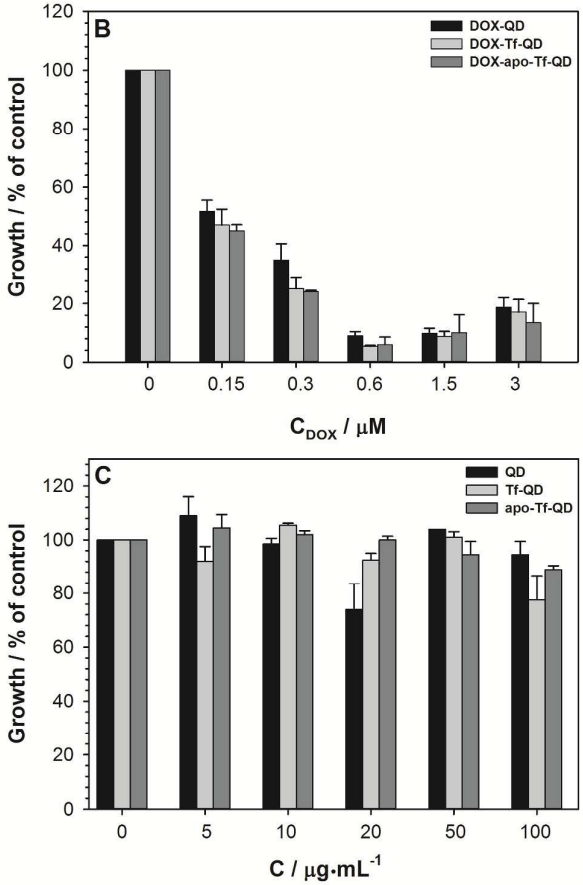

Fig. 6 Cytotoxicity of transferrin-nanoparticle nanoconjugates and doxorubicin-transferrin-nanoparticle nanoconjugates against human non-small cell lung carcinoma (H460 cells). (A)

View Article Online
DOI: 10.1039/C7NR07819F

Cytotoxic activity of DOX-QD, DOX-Tf-QD, DOX-apo-Tf-QD and free DOX against H460 cells expressed as IC_{50} value after 72 h of treatment, assessed by MTT assay. Data are expressed as mean ± SD of three independent experiments. (B) The growth inhibition of H460 cells with increasing concentrations of doxorubicin-transferrin-nanoparticle nanoconjugates following 72 h of incubation. Data are expressed as mean ± SD of three independent experiments. (C) Cytotoxicity of transferrin-nanoparticle nanoconjugates against H460 cells following 72 h of incubation. Data are expressed as mean ± SD of three independent experiments.

Conflicts of interest

There are no conflicts to declare.

Acknowledgements

This work was supported by a National Science Center of Poland Grant No. 2014/15/D/ST4/02989. We thank student Agata Zawistowska for assistance in spectroscopic experiments of Tf-QD. P.B. and A.P. want to acknowledge the support of NCN granting agency through the Grant No. 2015/17/B/ST4/03837.

Notes and references

1 R. A. Petros and J. M. DeSimone, *Nat. Rev. Drug Discovery* 2010, **9**, 615.
2 G. Hong, J. C. Lee, J. T. Robinson, U. Raaz, L. Xie, N. F. Huang, J. P. Cooke and H. Dai, *Nat. Med.*, 2012, **18**, 1841.
3 R. J. Clifford and J. H. Kaplan, *PLoS One*, 2013, **8**, e84306.
4 A. K. Das, *Ann. Med. Health Sci. Res.*, 2015, **5**, 93.
5 S. Kosugi, M. Hasebe, N. Matsumura, H. Takashima, E. Miyamoto-Sato, M. Tomita and H. Yanagawa, *J. Biol. Chem.*, 2009, **284**, 478.
6 R. Misra and S. K. Sahoo, *Europ. J. Pharm. Sci.*, 2010, **39**, 152.
7 J. Yu, X. Xie, M. Zheng, L. Yu, L. Zhang, J. Zhao, D. Jiang and X. Che, *Int. J. Nanomedicine*, 2012, **7**, 5079.
8 T.R. Daniels, T. Delgado, G. Helguera and M. L. Penichet, *Clin. Immunol.*, 2006, **121**, 159.
9 F. Okazaki, N. Matsunaga, H. Okazaki, N. Utoguchi, R. Suzuki, K. Maruyama, S. Koyanagi and S. Ohdo, *Cancer Res.*, 2010, **70**, 6238.
10 J. L. Heath, J. M. Weiss, C. P. Lavau and D. S. Wechsler, *Nutrients*, 2013, **5**, 2836.
11 Q. Y. He, A. B. Mason, R. C. Woodworth, B. M. Tam, R. T. MacGillivray, J. K. Grady and N. D. Chasteen, *Biochemistry*, 1997, **36**, 14853.
12 Y. Cheng, O. Zak, P. Aisen, S. C. Harrison and T. Walz, *Cell*, 2004, **116**, 565.
13 J. Wall, P. J. Halbrooks, C. Vonrhein, M. A. Rould, S. J; Everse, A. B. Mason and S. K. Buchanan, J. *Biol. Chem.*, 2006, **281**, 24934.
14 A. Bhattacharya, S. Chatterjee, V. Khorwal and T. K. Mukherjee, *Phys. Chem. Chem. Phys.*, 2016, ***18***, 5148.
15 L. B. Chen, F. Zhang and C. C. Wang, *Small*, 2009, **5**, 621.
16 H. Yukawa, R. Tsukamoto, A. Kano, Y. Okamoto, M. Tokeshi, T. Ishikawa, M. Mizuno and Y. Baba, *J. Cell Sci. Ther.*, 2013, **4**, 150.
17 Y. Cheng, A. C. Samia, J. D. Meyers, I. Panagopoulos, B. Fei and C. Burda, *J. Am. Chem. Soc.*, 2008, **130**, 10643.
18 L.-Y. Guan, Y.-Q. Li, S. Lin, M.-Z. Zhang, J. Chen, Z.-Y. Ma and Y.-D. Zhao, *Anal. Chim. Acta*, 2012, **741**, 86.
19 P. Zrazhevskiy, M. Sena and X. Gao, *Chem. Soc. Rev.*, 2010, **39**, 4326.
20 G. Palui, F. Aldeek, W. Wang and H. Mattoussi, *Chem. Soc. Rev.*, 2015, **44**, 193.
21 S. Goy-Lopez, J. Juarez, M. Alatorre-Meda, E. Casals, V. F. Puntes, P. Taboada and V. Mosqera, *Langmuir*, 2012, **28**, 9113.
22 S. Chakraborti, S. Sarwar and P. Chakrabarti, *J. Phys. Chem. B*, 2013, **117**, 13397.
23 A. Lesniak, F. Fenaroli, M. P. Monopoli, C. Aberg, K. A. Dawson and A. Salvati, *ACS Nano*, 2012, **6**, 5845.
24 S. Chatterjee and T. K. Mukherjee, *Phys. Chem. Chem. Phys.*, 2014, **16**, 8400.
25 A. M. Derfus, W. C. W. Chan and S. N. Bhatia, Probing the cytotoxicity of semiconductor quantum dots. *Nano Lett.*, 2004, **4**, 11.
26 L. Ye, K.-T. Yong, L. Liu, I. Roy, R. Hu, J. Zhu, H. Cai, W.-C. Law, J. Liu, K. Wang, J. Liu, Y. Liu, Y. Hu, X. Zhang, M. T. Swihart and P. N. A Prasad, *Nat. Nanotechnol.*, 2012, **7**, 453.
27 D. Aldakov, A. Lefrançois and P. Reiss, *J. Mater. Chem. C*, 2013, **1**, 3756.
28 P. Reiss, M. Carrière, C. Lincheneau, L. Vaure and S. Tamang, *Chem. Rev.*, 2016, **116**, 10731.
29 G. Xu, S. Zeng, B. Zhang, M. T. Swihart, K.-T. Yong and P. N. Prasad, *Chem. Rev.*, 2016, **116**, 12234.
30 P. Bujak, *Synth. Met.*, 2016, **222**, 93.
31 J. M. Klostranec and W. C. W. Chan, *Adv. Mater.*, 2006, **18**, 1953.
32 L. Li, T. J. Daou, I. Texier, T. T. K. Chi, N. Q. Liem and P. Reiss, *Chem. Mater.*, 2009, **21**, 2422.
33 P. Subramaniam, S. J. Lee, S. Shah, S. Patel, V. Starovoytov and K.-B. Lee, *Adv. Mater.*, 2012, **24**, 4014.
34 J.-Y. Chang, G.-Q. Wang, C.-Y. Cheng, W.-X. Lin and J.-C. Hsu, *J. Mater. Chem.*, 2012, **22**, 10609.
35 M. D. Regulacio, K. Y. Win, S. L. Lo, S.-Y. Zhang, X. Zhang, S. Wang, M.-Y. Han and Y. Zheng, *Nanoscal*e, 2013, **5**, 2322.
36 M. Z. Fahmi and J.-Y. Chang, *Nanoscale*, 2013, **5**, 1517.
37 D. Deng, J. Cao, L. Qu, S. Achilefu and Y. Gu, *Phys. Chem. Chem. Phys.*, 2013, **15**, 5078.
38 H. Shinchi, M. Wakao, N. Nagata, M. Sakamoto, E. Mochizuki, T. Uematsu, S. Kuwabata and Y. Suda, *Bioconjugate Chem.*, 2014, **25**, 286.
39 J. Song, C. Ma, W. Zhang, X. Li, W. Zhang, R. Wu, X. Cheng, A. Ali, M. Yang, L. Zhu, R. Xia and X. Xu, *ACS Appl. Mater. Interfaces*, 2016, **8**, 24826.
40 T.-T. Xuan, J.-Q. Liu, C.-Y. Yu, R.-J. Xie and H.-L. Li, *Sci. Rep.*, 2016, **6**, 24459.
41 T. Pons, E. Pic, N. Lequeux, E. Cassette, L. Bezdetnaya, F. Guillemin, F. Marchal and B. Dubertret, *ACS Nano*, 2010, **4**, 2531.
42 L. Li, R. Hu, I. Roy, G. Lin, L. Ye, J. L. Reynolds, J. Liu, J. Liu, S. A. Schwartz, X. Zhang and K.-T. Yong, *Theranostics*, 2013, **3**, 109.
43 L. Tan, S. Liu, X. Li, I. S. Chronakis and Y. Shen, *Colloids Surf. B*, 2015, **125**, 222.
44 Y. Ogihara, H. Yukawa, T. Kameyama, H. Nishi, D. Onoshima, T. Ishikawa, T. Torimoto and Y. Baba, *Sci. Rep.*, 2017, **7**, 40047.
45 G. Gabka, P. Bujak, K. Giedyk, A. Ostrowski, K. Malinowska, J. Herbich, B. Golec, I. Wielgus and A. Pron, *Inorg. Chem.*, 2014, **53**, 5002.

View Article Online
DOI: 10.1039/C7NR07819F

46 G. Gabka, P. Bujak, K. Kotwica, A. Ostrowski, W. Lisowski, J. W. Sobczak and A. Pron, *Phys. Chem. Chem. Phys.*, 2017, **19**, 1217.
47 Z. Liu, J. T. Robinson, X. Sun and H. Dai, *J. Am. Chem. Soc.*, 2008, **130**, 10876.
48 Z. Wang, P. Huang, A. Bhirde, A. Jin, Y. Ma, G. Niu, N. Neamati and X. Chen, *Chem. Commun.*, 2012, **48**, 9768.
49 Y. Wang, J. T. Chen and X. P. Yan, *Anal. Chem,* 2013, **85**, 2529.
50 A. G. Hovanessian and Z. L. Awdeh, *Eur. J. Biochem.,* 1976, **68**, 333.
51 G. Xu, R. Liu, O. Zak, P. Aisen and M. R. Chance, *Mol. Cell. Proteomics*, 2005, **4**, 1959.
52 A. Berczi, K. Barabas, J. A. Sizensky and W. P. Faulk, *Arch. Biochem. Biophys.* 1993, **300**, 356.
53 G. Gabka, P. Bujak, M. Gryszel, K. Kotwica and A. Pron, *J. Phys. Chem. C*, 2015, **119**, 9656.
54 A. M. Pyle, J. P. Rehmann, R. Meshoyrer, C. V. Kumar, N. J. Turro and J. K. Barton, *J. Am. Chem. Soc.*, 1989, **111**, 3051.
55 N. Li, Y. Ma, Ch. Yang, L. Guo and X. Yang, *Biophys. Chem.*, 2005, **116**, 199.
56 M. A. Komorowska and S. Olsztynska-Janus, *Biomedical Engineering, Trends, Research and Technologies*, InTech, Rijeka, 2011.
57 J. R. Lakowicz, Principles of fluorescence spectroscopy, Springer, Baltimore, 2010.
58 W. Zhong, J.-S. Yu, W. Huang, K. Ni and Y. Liang, *Biopolymers*, 2001, **62**, 315.
59 B. A. Wallace, *J. Synchrotron Rad.*, 2000, **7**, 289.
60 Z. M. Shen, J. T. Yang, Y.-M. Feng and Ch.-S. C. Wu, *Protein Sci.*, 1992, **1**, 1477.
61 F. Kilar and I. Simon, *Biophys. J.*, 1985, **48**, 799.
62 S. Krimm and J. Bandekar, *Adv. Protein Chem.*, 1986, **38**, 181.
63 J. Banker, *Biochim. Biophys. Acta*, 1992, **1120**, 123.
64 J. Kong and S. Yu, *Acta Biochim. Biophys. Sin.*, 2007, **39**, 549.
65 A.K. Saini, C.M. Carlin and H.H. Patterson, *J. Polym. Sci. A*, 1993, **31**, 2751.
66 M. Bodnar, J.F. Hartmann and J. Borbely, *Biomacromol.*, 2006, **7**, 3030.
67 L. Marin, E. Perju and D. Damaceanu, *Eur. Polym. J.*, 2011, **47**, 1284.
68 L. Marin, A. Zabulica and M. Sava, *Liq. Cryst.*, 2011, **38**, 433.
69 L. Marin, B. Simionescu and M. Barboiu, *Chem. Commun.*, 2012, **48**, 8778.
70 A. M. Oliveira-Brett, V. C. Diculescu and J. A. P. Piedade, *Bioelectrochem.*, 2002, **55**, 61.
71 A. M. Oliveira-Brett, J. A. P. Piedade, L. A. Silva and V. C. Diculescu, *Anal. Biochem.*, 2004, **332**, 321.
72 M. Potmesil, M. Izrael and R. Silber, *Biochem. Pharmacol.*, 1984, ***33***, 3137.
73 A. J. Birtle, *Clin. Oncol.*, 2000, **12**, 146.
74 A. Kowalczyk, A. M. Nowicka, M. Karbarz and Z. Stojek, *Anal. Bioanal. Chem.*, 2008, **392**, 463.
75 A. M. Nowicka, A. Kowalczyk, A. Jarzebinska, M. Donten, P. Krysinski, Z. Stojek, E. Augustin and Z. Mazerska, *Biomacromolecules*, 2013, **14**, 828.
76 J. W. Lowen, *Anthracycline and Anthracenechone Based Anticancer Agents*, Elsevier, Amsterdam, 1988.
77 J. D. McGhee and P. H. von Hippel, *J. Mol. Biol.*, 1974, **86**, 469.
78 M. Satyajit, J. F. Presley and F. R. Maxfield, *J. Cell. Biol.*, 1993, **121**, 1257.
79 F. R. Maxfield and T. E. McGraw, *Nat. Rev. Mol. Cell Biol.*, 2004, **5**, 121.
80 E. Augustin, B. Czubek, A. M. Nowicka, A. Kowalczyk, Z. Stojek, Z. Mazerska, *Toxicol. in Vitro*, 2016, **33**, 45.

View Article Online
DOI: 10.1039/C7NR07819F

TOC

Nanoconjugates of transferrin with alloyed quaternary nanocrystals (Tf-QD) can be considered as potential entities for the recognition of tumor cells.